Regular Article

INORGANIC CHEMISTRY RESEARCH
Published by the
Iranian Chemical Society
www.inorgchemres.org
info@inorgchemres.org

Inorg. Chem. Res., Vol. 5, No. 1, 37-49, June 2021
DOI: 10.22036/icr.2020.258236.1094

Sol-gel Synthesis of Selenium-doped Nickel Oxide Nanoparticles and Evaluation of their Cytotoxic and Photocatalytic Properties

Samaneh Ghazal[a], Alireza Akbari[a], Hasan Ali Hosseini[a], Zahra Sabouri[b], Mehrdad Khatami[c] and Majid Darroudi[d,e,*]

[a]*Chemistry Department, Payame Noor University, 19395-4697 Tehran, Iran*
[b]*Neurogenic Inflammation Research Center, Mashhad University of Medical Sciences, Mashhad, Iran*
[c]*Noncommunicable Diseases Research Center, Bam University of Medical Sciences, Bam, Iran*
[d]*Nuclear Medicine Research Center, Mashhad University of Medical Sciences, Mashhad, Iran*
[e]*Department of Medical Biotechnology and Nanotechnology, School of Medicine, Mashhad University of Medical Sciences, Mashhad, Iran*
(Received 20 November 2020, Accepted 22 December 2020)

In this paper, we examined the morphology, shape and magnetic and electronic properties of selenium-doped nickel oxide nanoparticles (Se-doped NiO-NPs), which were achieved through a sol-gel technique that involved the usage of Cydonia *oblonga* plant extract. The structural and magnetic properties of Se-doped NiO-NPs were evaluated by the employment of XRD, FESEM/EDAX, FT-IR, UV-Vis, and VSM procedures. According to XRD studies, the nanoparticles accommodated a face-centered cubic (fcc) crystalline structure and a space group of (*Fm3m*). In addition, the size of nanoparticles in optimal conditions (the optimum temperature of 400 °C and 3% Se-doped) were reported to be 7.7 nm while a direct relationship was also observed with increasing the concentration of selenium. The FESEM images confirmed the spherical morphology of Se-doped NiO-NPs. Also, the photocatalytic properties of Se-doped NiO-NPs were evaluated through the usage of methylene blue (MB) pigment degradation under UV light. The outcomes of this evaluation exhibited more than 76% of degrading within 200 min. To complete the project, the cytotoxicity aspect was also investigated on L929 cell lines, requiring the application of MTT assay, while the results were indicative of toxicity effects that can be used for inhibiting cancer cells.

Keywords: Se-doped NiO nanoparticles, Biosynthesis, Cydonia oblonga extract, Photocatalytic, Cytotoxicity

INTRODUCTION

Being a combination of technology and knowledge, the principal goal of nanotechnology is to control the materials or devices that contain a size of less than 100 nm [1]. Nanotechnology can be applied to a varying range of fields including materials engineering, medicine, semiconductor tools, pharmacy and drug design, electrical engineering, chemical engineering, and agricultural engineering [2,3]. The exertion of this knowledge can improve the properties of available products or even develop new products that contain novel features. In recent years, an extensive amount of research has been done on NiO-NPs since it has received the attention of many due to its significant mineral properties [4], as well as its magnetic, catalytic, and cathodic features that is vastly applied in industry [5]. Among the different methods that are available for synthesizing nanoparticles, the procedure of sol gel was selected for this work and performed through the usage of "*Cydonia oblonga*" plant extract [6], since it required a low-temperature and could be considered as an inexpensive method [7]. Among the advantages of exerting a sol-gel procedure for synthesizing nanoparticles, one could highlight the fact that the size of nanoparticles can be controlled or even duplicated with metal and non-metallic elements [8,9], while a uniformed dispersion of Dupont's

*Corresponding author. E-mail: darroudim@mums.ac.ir

would be observed throughout the final product. Furthermore, this method is applicable for the synthesis of ceramic materials and can be also exerted for the production of metal oxide thin films [10]. The obtained nanomaterials are capable of being vastly applied throughout the fields of electronics, medicine, separation technology, and optics [11]. NiO can be considered as a versatile semiconductor substance that contain a wide band gap with a range of 3.6-4.0 eV [12]. NiO-NPs have various applications such as the fabrication of electrochromic films [13], fuel cell electrodos [14], and gas sensors [15,16]; however, elemental doping stands as one of the factors that can enhance the implementation of synthesized nanoparticles [17] and in this regard, selenium can be highlighted as a perfect example. In this work, Se has been selected to be doped with NiO due to its appropriate chemical properties, as well as the simple fabrication of Se-doped NiO-NPs [18 19]. Selenium is a non-metal that is a necessity for health in small amounts but can be toxic in large volumes. This element is commonly found in composition and has been reported to be less pure in nature [20]. Consuming a massive amount of selenium can be toxic, however, an small portion that is mostly provided from food is needed for the cells to function [21]. Moreover, it is a powerful antioxidant that can prevent the harmful chemical reactions that occur throughout the body of cells [22,23], considering how supported cells are more capable of withstanding diseases such as heart disease, cancer, and age-related disorders [24]. The electrical conductivity of this element was detected to be low in dark and increase several times once positioned in brightness [22]. The most common utilization of selenium can be observed in electronics, photocopying, glasses, dyeing, rubber, metal alloys, textiles, photography, pharmaceuticals (antifungal shampoos), and medicine [25]. Although selenium is not taken as a physiologically essential ingredient in plants, however modern medical science considers this element to be an antioxidant and labels it as one of the essential nutrients required for the health of humans and animals [26,27]. Plants stand as the base of food production cycle in nature and their existence is quiet crucial for human and animal life, which consequently includes selenium as well [10,28].

The nanoparticles that are synthesized with the help of green chemistry laws can produce natural products, microorganisms, and polymer biomass, which can introduce a novel science and be added to the field of new nanotechnologies [2,29]. As it is known, green chemistry offers methods and products that are constructed, enhanced, and deployed to reduce or annihilate the factors that threaten the health of humans or environment [30-32]. The ultimate goal of this particular chemistry is to improve the quality of life on a cleaner and safer planet [33]. Se-doped NiO-NPs were prepared at different concentrations of selenium including (1%), (3%) and (5%) at the optimum temperature of 400 ℃ [34,35]. Thereafter, the cytotoxicity and photocatalytic activities of these nanoparticles were assessed to complete the report. One of the highlights of this project is the utilization of least possible amount of Se-doped NiO-NPs in the role of catalyst (3.0 mg), which was performed under UVA-light with a low-intensity (11W) [36,37]. Taking these conditions into consideration, the percentage of MB degradation was observed to be around 76% under UVA light subsequent to 200 min [38-40]. Also, the cytotoxicity of these nanoparticles was evaluated on L929 cell lines, which had required the application of MTT assay [41]. In order to complete the process, the characterization of synthesized Se-doped NiO-NPs was carried out by the usage of FT-IR, XRD, UV-Vis, FESEM/EDAX and VSM methods [42,43].

SYNTHESIS OF SE-DOPED NIO-NPS

Materials

The chemical materials in this experiment were tested without further purification. Double-distilled water, $Ni(NO_3)_2 \cdot 6H_2O$ (Merck, Germany) (99.9%), the plant extract of *Cydonia oblonga*, and $Na_2Se_2O_3$ (Merck, Germany) (99.9%) were selected as the basis of nickel, coating agent, and basis of selenium, respectively.

Production of Cydonia Oblonga Extract

In order to prepare the extract of *Cydonia oblonga*, about 1.0 g of the seed was poured into 200 mL of double-distilled water and covered for 24 h at room temperature. The obtained extract was filtered afterwards and maintained at 4 °C.

Synthesis of Se-doped NiO-NPs

In this study, Se-doped NiO-NPs were prepared using

Fig. 1. The synthesis schematic of Se-doped NiO-NPs.

of sol-gel method at various concentrations along with following the form of $Se_xNi_{(1-x)}O$. To calculate the content of nitrate, the formulas of 0.087 (Se 1% wt.%), 0.261 (Se 3% wt.%) and 0.435 g of ($Na_2Se_2O_3$) (Se 5% wt.%) were applied subsequent to being dissolved in 100 mL of double-distilled water and stirred for the duration of 30 min. Moreover, for the purpose of preparing NiO-NPs, 14.54 g of $Ni(NO_3)_2.6H_2O$ (0.50 M) was dissolved in 100 mL of double-distilled water and stirred for a period of 30 min. In order to attain a homogenous solution, the $Na_2Se_2O_3$ solution was added to the (Ni $(NO_3)_2.6H_2O$) solution, while later on 20 mL of *Cydonia oblonga* extract solution was appended drop wisely to the mixture solution under constant stirring. As the next step, the container that held the solutions was transferred into an oil bath and stirred at 80 °C for 12 h. The obtain gel after completing this process was calcinated at 400 °C for 2h, resulting in achieving black Se-doped NiO-NPs. The synthesizing schematic of Se-doped NiO-NPs is presented in Fig. 1.

Characterization

The biosynthesis of Se-doped NiO-NPs was analyzed through the usage of various techniques such as UV-Vis, FT-IR, XRD, FESEM/EDAX and VSM. In addition, their optical features were measured as well through the utilization of a UV-Vis spectrophotometer (Shimadzu, model UV-1800) and the results were observed to range starting from 200 and reach up to 800 nm. In the following, the obtained nanoparticles were identified with FESEM and EDX analysis. (TESCAN BRNO-Mira3 model), while their crystal structure had been distinguished through the usage of XRD pattern (model, D8-Advance Bruker). The nanoparticles were measured by FT-IR (FT-IR) spectra (8400-SHIMADZU made in Germany) for the purpose of identifying the existing bonds and functional groups throughout the range of 4000-400 cm^{-1}. Lastly, the magnetic properties of obtained Se-doped NiO-NPs were investigated by the application of VSM (model MDKB).

RESULTS AND DISCUSSION

XRD Pattern

Figure 2 offers the structural and crystalline information of Se-doped NiO-NPs that were taken in different concentrations at the temperature of 400 °C. The perceivable distributed peaks around the 2θ degrees (within

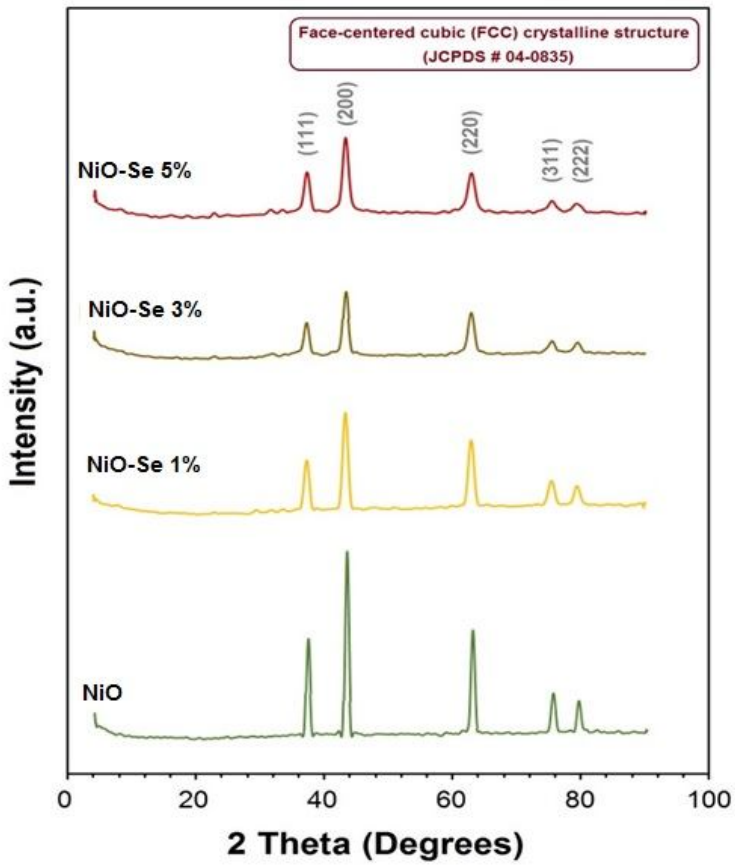

Fig. 2. The XRD patterns of fabricated Se-doped NiO-NPs.

the range of 35-85°) appear to be (111), (200), (220), (222) and (311), being indicative of the crystal structure of NiO-NPs biosynthesis that were in the form of face cube axis (fcc) [44]. It is notable that the crystal sheets were quite comparable to those of the NiO (JCPDS # 04-0835) [45]. The purity of synthesized nanoparticles was confirmed through the lack of observing any other peaks in this spectrum. According to the reports, a decrease in the peak intensity can be caused by increasing the concentration of selenium, which leads to an enlargement in the crystallite size [46]. This enlargement could be related to the induced increase within the internal structural weakens that results in heightening the rate of growth [47,48]. Considering this fact, it can be concluded that the peaks of nanoparticles are less extensive than the ordinary materials and consequently, the size of synthesized nanoparticles can cause different effects on biological activities [49,50]. The crystallite size was calculated by applying Debye-Scherrer formula (Eq. (1)) and results are presented in Table 1 [11,51].

$$D = k\lambda/(\beta\cos\theta) \quad (1)$$

where, k = 0.9, D would be the size of crystallite, λ stands as the wavelength of X-ray, β is the FWHM relative to the XRD peaks, and θ would be the diffraction angle.

FTIR

Figure 3 presents the FT-IR spectrum of bare NiO-NPs and Se-doped NiO-NPs in three different concentrations at the optimum temperature of 400 °C, which is available in the range of 400-4000 cm^{-1}, and were achieved by the utilization of *Cydonia oblonga* extract. For this purpose, the

Table 1. Comparison of Particle Size of the Se-doped NiO-NPs

Selenium percentage	2θ (deg.)	FWHM (rad.)	Diameter (nm)	Identification
0% (Un-doped NiO-NPs)	43.3	0.009	16.5	fcc (NiO)
1%	43.41	1.26	7.4	fcc (NiO + Se)
3%	43.27	1.15	7.7	fcc (NiO + Se)
5%	43.34	1.03	8.2	fcc (NiO + Se)

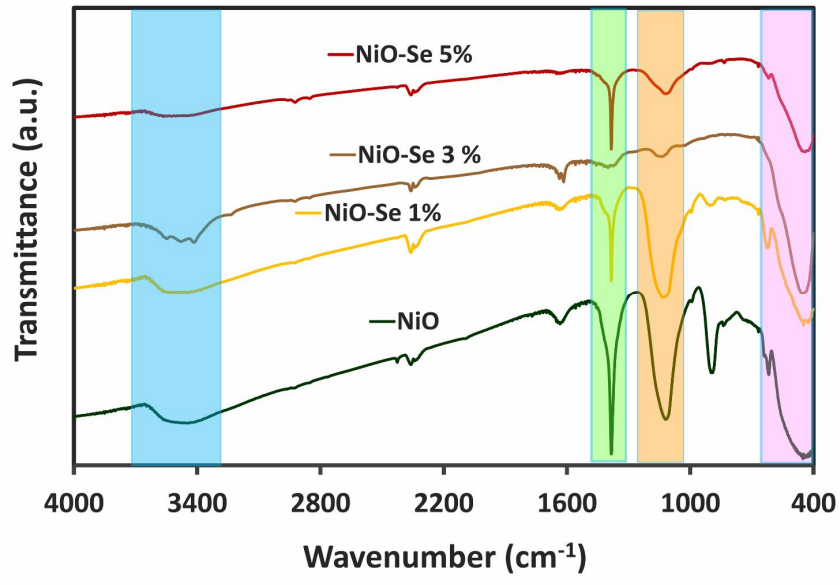

Fig. 3. The FTIR spectra of fabricated Se-doped NiO-NPs.

powdered samples were mixed with KBr and resulted in exhibiting wide bands throughout the region of 4000 to 400 cm^{-1}. It can be indicated from the FTIR spectrum that the existing broadband at the point of 3400 cm^{-1} was associated with the O-H stretching vibrations of water molecules [8,52] that were either caused by the presence of water in KBr or the liquid that was adsorbed by NiO-NPs. Furthermore, the observed band within the zone of 2300 is apparently related to the CO_2 molecules of the air [53], while the sharp band present in 1385 cm^{-1} indicates the tensile vibration of N=O that was created by the existing small amount of nitrate [54,55]. The other band that can be observed at 1616 cm^{-1} is attributed to the bending vibrations that are produced by water molecules [56]. And the observed peak at 400 to 450 cm^{-1} is related to the existing bond between Ni-O. It is also notable that according to the

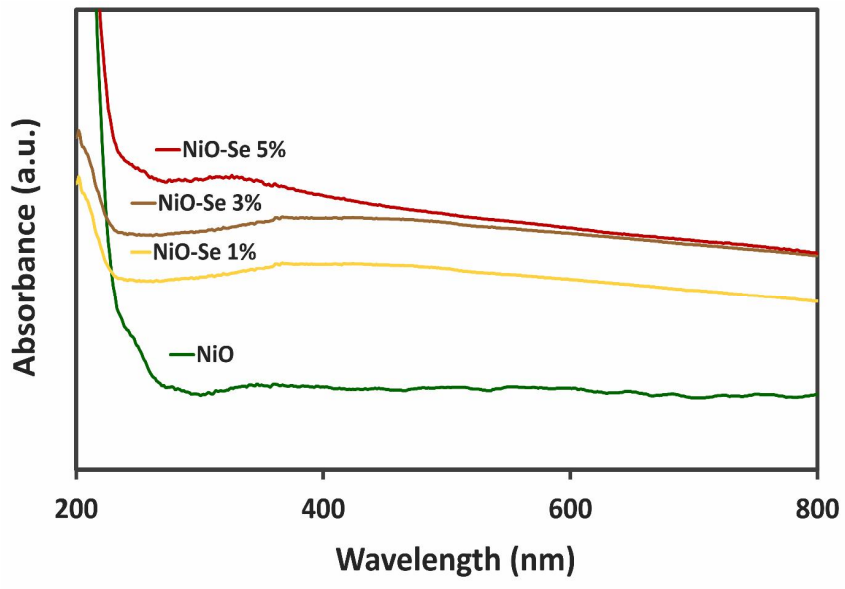

Fig. 4. The UV-Vis spectra of prepared Se-doped NiO-NPs.

achieved data, the severity of peaks faced a reduction as the concentration of selenium was increased.

UV-Vis Spectrum

The UV-Vis spectrum of pure NiO-NPs and Se-doped NiO-NPs that were obtained by the usage of *Cydonia Oblonga* extract in three different concentrations at a wavelength of 200-800 nm is presented in Fig. 4. The inducement of an electron transfer that had occurred from the valence band towards the conduction band ($O_2p \rightarrow Ni_3d$) resulted in observing an absorption band within the region of 310 to 340 nm in regards to NiO and Se-doped NiO-NPs [57,58]. The optical absorption of Se-doped NiO-NPs is dependent on a variety of factors including the particle size and energy gap [59,60]. The obtained data indicated that by increasing the size of particles, the amount of light absorption could be forced to face a reduction [54,60].

FESEM/EDAX/PSA

The FESEM, EDAX and PSA pictures of Se-doped NiO-NPs in three concentrations (1%, 3% and 5%) at the temperature of 400 °C is illustrated in Figs. 5a-o. As it can be observed, there is a 5% increase in the coverage categories that contain the Se content, which is suggestive of a higher compression throughout the nanoparticles that were doped at 5% Se [61]. According to Figs. 5a-k, the morphology of all the synthesized nanoparticles was spherical while being uniformly distributed. There was an even further compression of nanoparticles that were released at 5% selenium, which was confirmed by the coating classification with selenium content increased to 5%. These results can be taken as a proof to highlight the major role of contaminated selenium concentration in separating the synthesized nanoparticles. Furthermore, the histogram curves that are presented in Figs. 5d, h and l identify the distribution of nanoparticles and as it can be perceived, the average size of nanoparticles faced an increase from 59.2 to 84.5 nm as the selenium concentration was intensified from 1 to 5 percent. This data is comparable to the outcomes of XRD model and signifies the non-agglomerated situation of NiO-NPs. Figures 5m, n and O exhibits the interpretation of EDX spectra that have confirmed the presence of nickel and selenium elements [62]. The FESEM images are also consistent with the XRD results and thoroughly define the particle size [63].

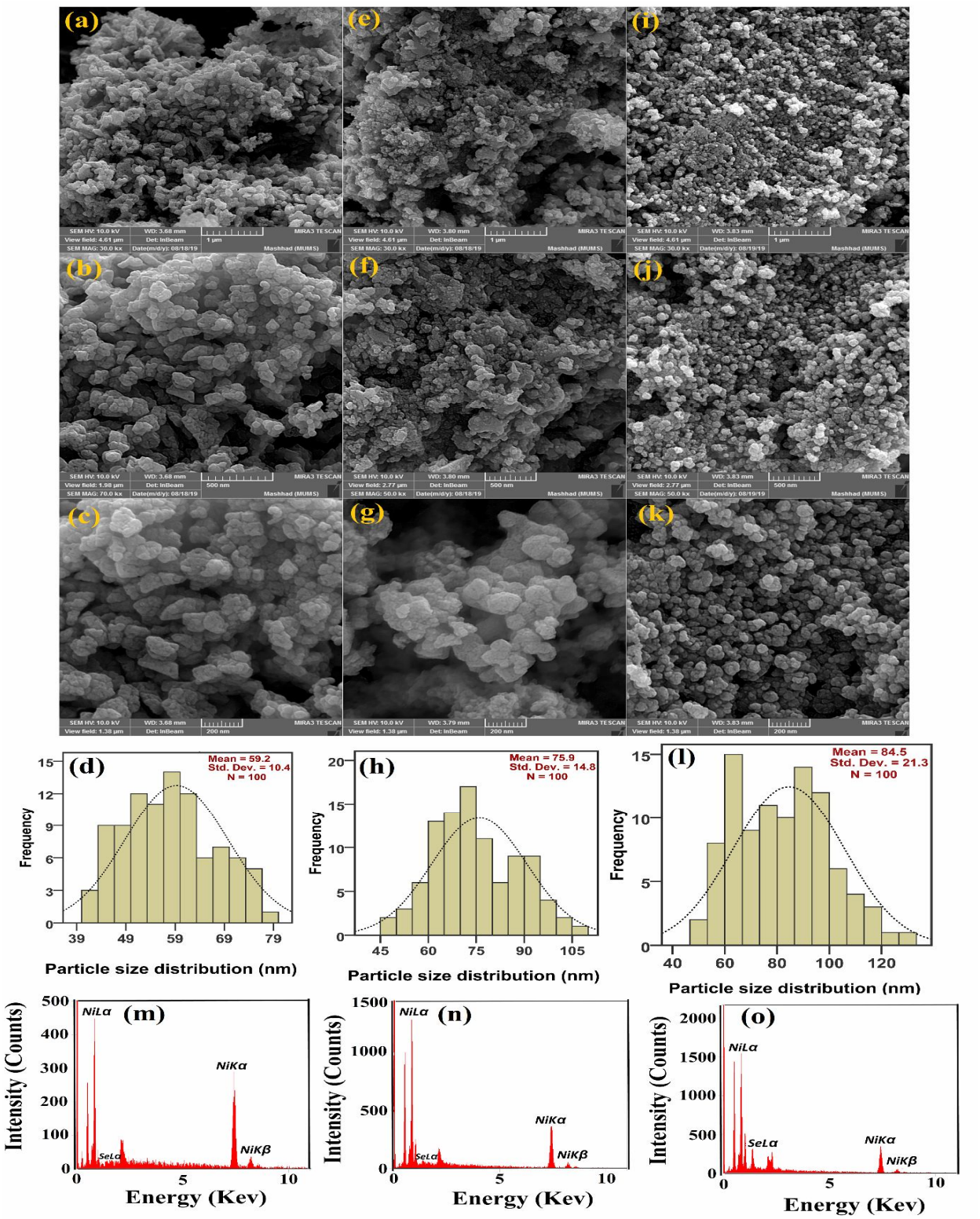

Fig. 5. The FESEM images in three concentrations (1%, 3% and 5%) and scales (1 µ, 500 nm, and 200 nm) (a-k) and PSA curves (200 nm) (d-l) and EDX analyze (m-o) of Se-doped NiO-NPs.

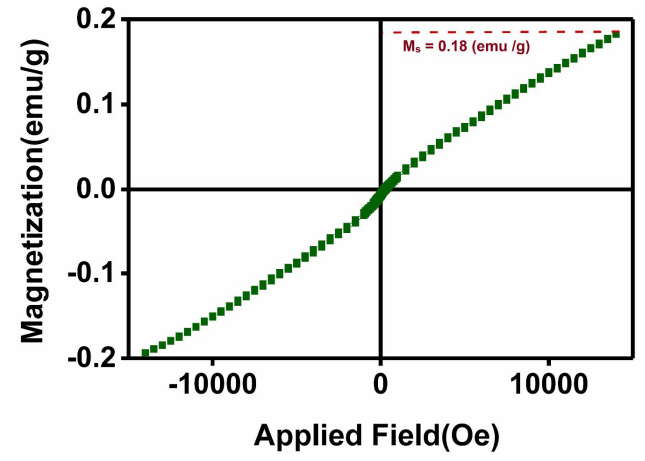

Fig. 6. VSM curve of the Se-doped NiO-NPs (Se 3%) at the temperature of 400 °C.

VSM

The magnetization behaviors of Se-doped NiO-NPs (Se 3%) at the temperature of 400 °C are illustrated in Fig. 6 and as it can be observed, we arranged the magnetic field to sweep from -10,000 to +10,000 Oe. According to the data, the saturation magnetization (Ms) of Se-doped NiO was reported to be 0.18 emu/g, Magnetization in the case of NiO-NPs seemed to linearly increase ,while saturation was not perceived to face any alteration as the magnetic intensity was heightened Up to 10,000 Oe. This result could be due to the electronic arrangements from uncompensated spins on the sample surface, indicating the presence of antiferromagnetic behavior [64]. Next to having comparable results with our findings, the work of G. Bharathy [65] demonstrated the capability of selenium in functioning as a control agent of nanoparticles sizes and increasing the magnetic saturation (M_S) of nanoparticles [66]. Considering the size of Se-doped NiO-NPs with the average diameter of about 7.7 nm, it can be assumed that they only contain one single magnetic domain [67,68].

Photocatalytic Activity

The utilization of MB compound and exposure to UV-A light was required in order to perform the photocatalytic procedure of Se-doped NiO-NPs (Se 3%) at pH = 9 and accordingly, exerted photocatalytic decomposition by the means of UV-A radiation. Science has labeled MB dye as a conventional pollutant and a serious imminence for the health of humans, which commonly exists throughout water-free regions; as it is known, this pollutant is fabricated by industrialized dying operations. To begin the procedure, 50 mL of MB solution (10^{-5} M) was initially prepared and afterwards, the absorption of MB solution was measured in the range of 200-800 nm. First, around 3 mg of Se-doped NiO-NPs was added to the MB solution and stirred in dark for 30 min for reaching an adsorption-desorption equilibrium. Once the absorbance of the solution had been noted [69], it was required to expose the sample to UV-A light in ambient temperature. Meanwhile, the absorption and degradation rates had to be taken down in various stages along with intervals of 25 min. The destruction percentage of MB was calculated by the application of Eq. (2), being reported to be about 76% after 200 min [65].

$$Degradation\ (\%) = \frac{A_0 - A_t}{A_0} \times 100 \qquad (2)$$

(A_0 would be the absorbance of the solution in prior to UV-irradiation and A_t stands for the absorbance of the solution at any instant). Figure 7a exhibits the MB degradation that was achieved through the usage of Se-doped NiO-NPs (Se 3%) and the involvement of UV-irradiation [70,71]. Various mechanisms for the photocatalytic activities of Se-doped NiO-NPs have been proposed such as the following [72,73]. If the UVA light energy is equaled to or

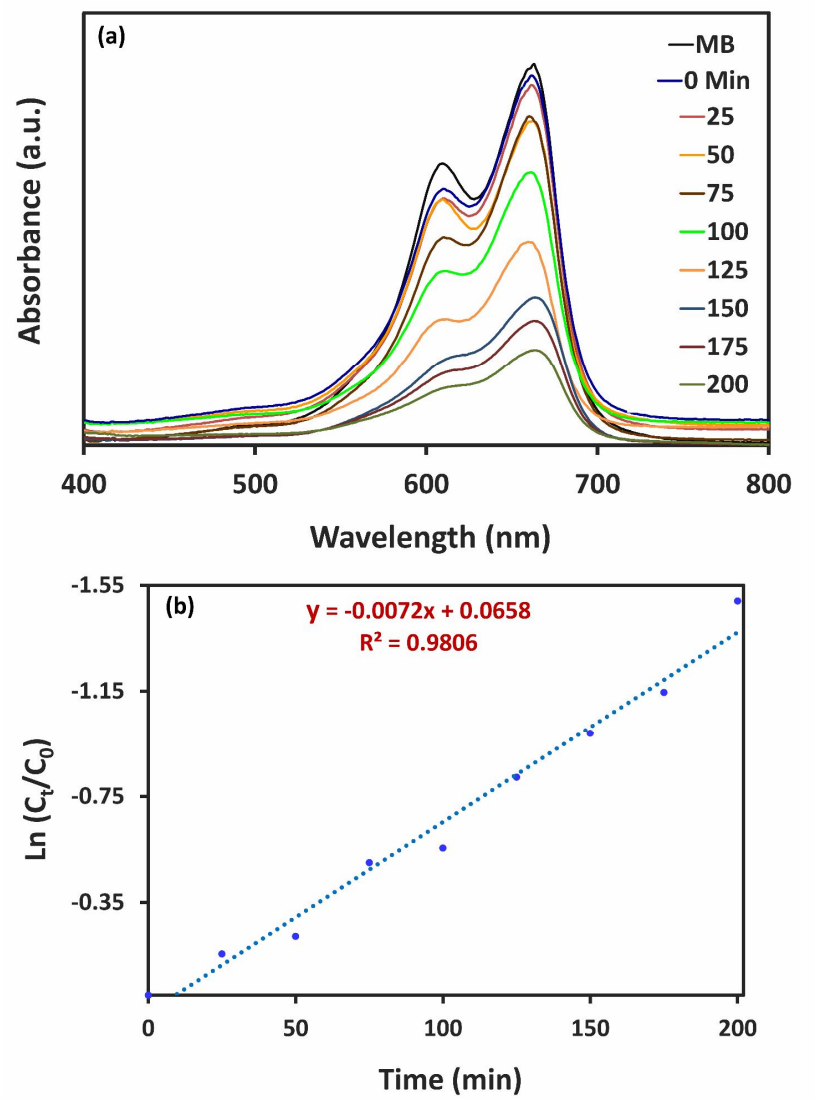

Fig. 7. Degradation of MB under UV-irradiation.

greater than the band gap energy of the nanoparticles, the electrons are excited from the valance band (VB) to the conduction band (CB) [74]. In this process, the fabrication of holes in capacitance band and electrons in conduction band can be observed.

In most of the cases, the hole on the surface of Se-doped NiO-NPs reacts with water molecules to produce hydroxyl radicals (OH°), while the conduction band electron (eCB^-) reacts with electron acceptors such as oxygen (O_2) and anion radicals for product superoxide radical anion ($^{0}O_2^-$) (reactions 1 to 6).

$$h\nu\,(UV) + Se-doped\ NiO \rightarrow Se-doped\ NiO^{*} + h^{+} + e^{-} \quad (1)$$

$$Se-doped\ NiO\,(h^{+}) + H_2O \rightarrow Se-doped\ NiO + H^{+} + OH^{\circ} \quad (2)$$

$$Se-doped\ NiO\,(e^{+}) + O_2 \rightarrow Se-doped\ NiO + {}^{\circ}O_2^{-} \quad (3)$$

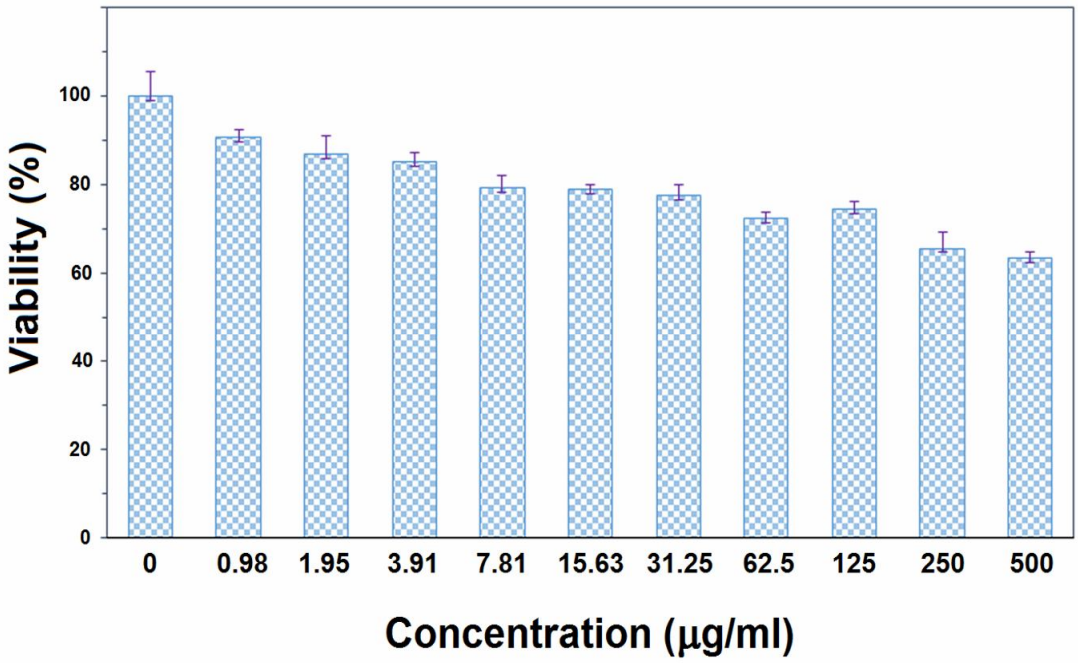

Fig. 8. Cytotoxicity investigation of Se-doped NiO-NPs using MTT assay.

$$Dye + {}^{\circ}OH \rightarrow Degradation\ product \quad (4)$$

$$Dye + h^{+} \rightarrow Oxidation\ products \quad (5)$$

$$Dye + e^{-} \rightarrow \mathrm{Re}duction\ products \quad (6)$$

These reactions prevent electrons and holes from recombining. OH° and ${}^{0}O_2^{-}$ that are formed according to the above reactions, react with the organic molecule and decompose the organic compound after creating intermediate products.

Photocatalytic Kinetics

Figure 7b demonstrates the kinetic graphical degradation of MB pigment, in which Se-doped NiO-NPs (Se 3%) were displayed to UV-A light. According to the obtained results, 0 to 200 min is the time needed to fulfill the photocatalytic procedure, which is accompanied with the time intervals of 25 min. Furthermore, it was determined by Eq. (3) that the kinetic reaction follows the first order model [75,76].

$$\ln\left(\frac{C_t}{C_0}\right) = K_{obs}\, t \quad (3)$$

Where C_0 represents the concentration of solution in prior to light, C_t would be the concentration of solution at any moment, and K_{obs} stands for the detected rate of constant that is parallel to -0.007 min^{-1} [77,78].

Cytotoxicity of Se-doped NiO-NPs

In this section, the cytotoxicity of Se-doped NiO-NPs was evaluated on the growth and production of human Glioblastoma cancer (L929) cell lines by the MTT method (3-(4,5-dimethylthiazol-2-yl)-2,5-diphenyl tetrazolium bromide) [30,48]. Being based on living cells, the decomposition of tetrazolium salt through the effects of mitochondrial enzyme succinate dehydrogenase mitochondria plays a crucial part in this competitive mitochondrial metabolic procedure. Initially, 100 µL of the culture medium that was consisted of 1×10^4 cells/well was placed in a 96-well plate. Once 24 h of incubation had passed, various concentrations of Se-doped NiO-NPs (0 to 500 µg mL^{-1}) was added to the cells and incubated for another round of 24 h. In the following, every single well plate was injected with 20 µL of MTT that contained a volume of 0.5 mg mL^{-1} and incubated in dark for a period of

4 h at 37 °C. The next step was to carefully extract the MTT culture medium and have 100 µL of DMSO mixed with each of the plates in order to disperse the fabricated purple formaldehyde [79]. Lastly, the amount of light absorption was measured by the means of a microplate reader at 545 nm [80]. As it is indicated by Fig. 8, the results of laboratory cell toxicity examinations were thoroughly summed up after being incubated for 24 h by including different amounts of nanoparticles within the range of 0-500 µg mL^{-1}. According to these outcomes, the synthesized nanoparticles have exhibited toxicity effects while containing the potential of being exerted for inhibiting cancer cells.

CONCLUSIONS

In this paper, Se-doped NiO-NPs were synthesized by the usage of *Cydonia Oblonga* extract in three different concentrations (*e.g.*, 1, 3 and 5%) of selenium at the optimum temperature of 400 °C. These nanoparticles were subjected to various analyzes that include UV-Vis, FT-IR, XRD, FESEM/EDAX and VSM. In accordance with the XRD observations, the size of nanoparticles faced an increase as the selenium concentration was extended from (1 to 5%). Also, the obtained results from VSM examination were indicative of the antiferromagnetic properties of these nanoparticles, while their spherical shape was proved via FESEM pictures. Moreover, the outcomes of MTT assay in regards to the included cell lines (L929) demonstrated the cytotoxicity effect of Se-doped NiO-NPs. The gathered Photocatalytic results confirmed the capability of Se-doped NiO-NPs in functioning as photocatalyst during the process of MB degradation under UV light. Accordingly, it was observed that the degradation percentage of MB was about 76% under UV irradiation. Hence, Se-doped NiO-NPs can be identified as an effective catalyst for being applied in wastewater treatment since they exhibited an excellent performance in eliminating the appointed pollutants.

ACKNOWLEDGMENTS

The technical support of this project was provided by Payame Noor University of Mashhad and Mashhad University of Medical Sciences based on the thesis of Mrs. S. Ghazal.

REFERENCES

[1] K. Beers, D. Sur, G.B. Basim, MRS Adv. 5 (2020) 2209.
[2] J. Shi, G. Ni, J. Tu, X. Jin, J. Peng, J. Nanopart. Res. 19 (2017) 209.
[3] B. Pelaz, C. Alexiou, R.A. Alvarez-Puebla, F. Alves, A.M. Andrews, S. Ashraf, L.P. Balogh, L. Ballerini, A. Bestetti, C. Brendel, ACS Publ. 2017.
[4] G. Kavitha, K.T. Arul, P. Babu, J. Mater. Sci.: Mater. Electron. 29 (2018) 6666.
[5] N. Xu, S.E. Huq, J. Mater. Sci. Eng. Rep. 48 (2005) 47.
[6] W. Yu, H. Xie, J. Nanomater. 2012 (2012) 435873.
[7] Y. Huang, Y. Zhang, S. Lin, L. Yan, R. Cao, R. Yang, X. Liang, W. Xiang, J. Alloys Compd. 686 (2016) 564.
[8] Z. Sabouri, A. Akbari, H.A. Hosseini, M. Darroudi, J. Mol. Struct. 1173 (2018) 931.
[9] E. Matijevic, Google Patents, 1991.
[10] F. Thema, E. Manikandan, A. Gurib-Fakim, M. Maaza, J. Alloys Compd. 657 (2016) 655.
[11] V. Benitha, K. Jeyasubramanian, R. Mala, G. Hikku, R.R. Kumar, J. Coat. Technol. Res. 16 (2019) 59.
[12] H. Sato, T. Minami, S. Takata, T. Yamada, Thin Solid Films 236 (1993) 27.
[13] V.M. Shajudheen, M. Sivakumar, S.S. Kumar, Mater. Today: Proc. 3 (2016) 2450.
[14] F. Li, H.-Y. Chen, C.-M. Wang, K.-A. Hu, J. Electroanal. Chem. 531 (2002) 53.
[15] I. Hotovy, J. Huran, L. Spiess, S. Hascik, V. Rehacek, Sens. Actuators, B: Chem. 57 (1999) 147.
[16] S. Ekambaram, M. Maaza, J. Alloys Compd. 395 (2005) 132.
[17] M.S. Shatalov, R. Gaska, J. Yang, M. Shur, Google Patents, 2016.
[18] G. Tarancon III, Google Patents, 2014.
[19] K. Kaviyarasu, E. Manikandan, J. Kennedy, M. Jayachandran, R. Ladchumananandasiivam, U.U. De Gomes, M. Maaza, Ceram. Int. 42 (2016) 8385.
[20] B. Abraham, S. Uba, I. Abdulkadir, ATBU J. Sci. Educ. Technol. 4 (2016) 122.

[21] G.F. Combs, Br. J. Nutr. 85 (2001) 517.
[22] R. Aversa, R.V. Petrescu, A. Apicella, F.I. Petrescu, J. Eng. Appl. Sci. 9 (2016) 1189.
[23] A.T. Khalil, M. Ovais, I. Ullah, M. Ali, Z.K. Shinwari, M. Maaza, Arabian J. Chem. 13 (2020) 606.
[24] P. Lang, W. Mitchell, A. Lapenna, D. Pitts, R. Aspinall, Eur. Geriatr. Med. 1 (2010) 112.
[25] J. Köhrle, J. Trace Elem. Med. Biol. 18 (2004) 61.
[26] K. Soetan, C. Olaiya, O. Oyewole, Afr. J. Food Sci. 4 (2010) 200.
[27] N. Mayedwa, N. Mongwaketsi, S. Khamlich, K. Kaviyarasu, N. Matinise, M. Maaza, Appl. Surf. Sci. 446 (2018) 250.
[28] Y.-G. Zhu, E.A. Pilon-Smits, F.-J. Zhao, P.N. Williams, A.A. Meharg, Trends Plant Sc. 14 (2009) 436.
[29] M. Darroudi, M.B. Ahmad, A.H. Abdullah, N.A. Ibrahim, K. Shameli, Int. J. Mol. Sci. 11 (2010) 3898.
[30] K. Sravanthi, D. Ayodhya, P.Y. Swamy, Mater. Sci. Energy Technol. 2 (2019) 298.
[31] A. Diallo, E. Manikandan, V. Rajendran, M. Maaza, J. Alloys Compd. 681 (2016) 561.
[32] N. Matinise, K. Kaviyarasu, N. Mongwaketsi, S. Khamlich, L. Kotsedi, N. Mayedwa, M. Maaza, Appl. Surf. Sci. 446 (2018) 66.
[33] P. Anastas, J. Warner, Oxford University Press, Inc., New York, 1998.
[34] K. Lokesh, G. Kavitha, E. Manikandan, G.K. Mani, K. Kaviyarasu, J.B.B. Rayappan, R. Ladchumananandasivam, J.S. Aanand, M. Jayachandran, M. Maaza, IEEE Sens. J. 16 (2016) 2477.
[35] B. Sone, X. Fuku, M. Maaza, Int. J. Electrochem. Sci. 11 (2016) 8204.
[36] A. Raza, M. Ikram, M. Aqeel, M. Imran, A. Ul-Hamid, K.N. Riaz, S. Ali, Appl. Nanosci. (2019) 1.
[37] A. Rafiq, M. Imran, M. Aqeel, M. Naz, M. Ikram, S. Ali, J. Inorg. Organomet. Polym. Mater. 30 (2020) 1915.
[38] D. Rani Rosaline, S. Inbanathan, A. Suganthi, M. Rajarajan, G. Kavitha, R. Srinivasan, H. Hegazy, A. Umar, H. Algarni, E. Manikandan, J. Nanosci. Nanotechnol. 20 (2020) 924.
[39] M. Aqeel, A. Rafiq, H. Majeed, S. Ali, Nanoscale Res. Lett. 15 (2020) 75.
[40] M. Junaid, M. Imran, M. Ikram, M. Naz, M. Aqeel, H. Afzal, H. Majeed, S. Ali, Appl. Nanosci. 9 (2019) 1593.
[41] A.T. Khalil, M. Ovais, I. Ullah, M. Ali, Z.K. Shinwari, D. Hassan, M. Maaza, Artificial Cells, Artif. Cells, Nanomed., Biotechnol. 46 (2018) 838.
[42] T.A. Nguyen, L.T.T. Nguyen, V.X. Bui, D.H. Nguyen, H.D. Lieu, L.M. Le, V. Pham, J. Alloys Compd. 103 (2020) 155098.
[43] A. Zhukov, M. Ipatov, C. Garcia, M. Churyukanova, S. Kaloshkin, V. Zhukova, Appl. Phys. A 115 (2013) 547.
[44] P.M. Kibasomba, S. Dhlamini, M. Maaza, C.-P. Liu, M.M. Rashad, D.A. Rayan, B.W. Mwakikunga, Results Phys. 9 (2018) 628.
[45] G. Tong, Q. Hu, W. Wu, W. Li, H. Qian, Y. Liang, J. Mater. Chem. 22 (2012) 17494.
[46] R.K. Das, A.K. Golder, J. Electroanal. Chem. 823 (2018) 9.
[47] L. Ouarez, A. Chelouche, T. Touam, R. Mahiou, D. Djouadi, A. Potdevin, J. Lumin. 203 (2018) 222.
[48] B. Ngom, T. Mpahane, N. Manyala, O. Nemraoui, U. Buttner, J. Kana, A. Fasasi, M. Maaza, A. Beye, Appl. Surf. Sci. 255 (2009) 4153.
[49] Z. Sabouri, N. Fereydouni, A. Akbari, H.A. Hosseini, A. Hashemzadeh, M.S. Amiri, R.K. Oskuee, M. Darroudi, Rare Met. 39 (2020) 1134.
[50] A.T. Khalil, M. Ovais, I. Ullah, M. Ali, Z.K. Shinwari, S. Khamlich, M. Maaza, Nanomed. 12 (2017) 1767.
[51] H. Yan, D. Zhang, J. Xu, Y. Lu, Y. Liu, K. Qiu, Y. Zhang, Y. Luo, Nanoscale Res. Lett. 9 (2014) 424.
[52] Z. Sabouri, A. Akbari, H.A. Hosseini, A. Hashemzadeh, M. Darroudi, J. Mol. Struct. 1191 (2019) 101.
[53] K. Sathishkumar, N. Shanmugam, N. Kannadasan, S. Cholan, G. Viruthagiri, Mater. Sci. Semicond. Process. 27 (2014) 846.
[54] M. Gondal, T.A. Saleh, Q. Drmosh, Appl. Surf. Sci. 258 (2012) 6982.
[55] P. Vishnukumar, B. Saravanakumar, G. Ravi, V. Ganesh, R.K. Guduru, R. Yuvakkumar, Mater. Lett. 219 (2018) 114.

[56] Z. Sabouri, A. Akbari, H.A. Hosseini, A. Hashemzadeh, M. Darroudi, J. Cluster Sci. 30 (2019) 1425.

[57] M. Darroudi, M. Ahmad, R. Zamiri, A. Abdullah, N. Ibrahim, A. Sadrolhosseini, Solid State Sci. 13 (2011) 520.

[58] Z. Sabouri, A. Akbari, H.A. Hosseini, M. Khatami, M. Darroudi, Bioprocess Biosyst. Eng. 43 (2020) 1209.

[59] M. Darroudi, M.B. Ahmad, A.K. Zak, R. Zamiri, M. Hakimi, Int. J. Mol. Sci. 12 (2011) 6346.

[60] S. Karthik, P. Siva, K.S. Balu, R. Suriyaprabha, V. Rajendran, M. Maaza, Adv. Powder Technol. 28 (2017) 3184.

[61] A.J. Christy, M. Umadevi, Mater. Res. Bull. 48 (2013) 4248.

[62] S. Senobari, A. Nezamzadeh-Ejhieh, J J. Mol. Liq. 261 (2018) 208.

[63] S.Z. Khan, Y. Yuan, A. Abdolvand, M. Schmidt, P. Crouse, L. Li, Z. Liu, M. Sharp, K. Watkins, J. Nanopart. Res. 11 (2009) 1421.

[64] B. Gokul, P. Saravanan, V. Vinod, M. Černík, R. Sathyamoorthy, Powder Technol. 274 (2015) 98.

[65] S. Ghazal, A. Akbari, H.A. Hosseini, Z. Sabouri, F. Forouzanfar, M. Khatami, M. Darroudi, Appl. Phys. A 126 (2020) 480.

[66] R. Suresh, V. Ponnuswamy, C. Sankar, M. Manickam, S. Venkatesan, S. Perumal, J. Magn. Magn. Mater. 441 (2017) 787.

[67] S. Baran, A. Hoser, B. Penc, A. Szytuła, Acta Phys. Pol., A 129 (2016) 35.

[68] A. Rajesh, M.M. Raja, K. Gurunathan, Acta Metall. Sin. (Engl. Lett.) 27 (2014) 253.

[69] O. Omotunde, A. Okoronkwo, A. Aiyesanmi, E. Gurgur, J. Photochem. Photobiol., A 365 (2018) 145.

[70] M. Ali, S. Sharif, S. Anjum, M. Imran, M. Ikram, M. Naz, S. Ali, Mater. Res. Express 6 (2020) 1250d1255.

[71] M. Ikram, J. Hassan, M. Imran, J. Haider, A. Ul-Hamid, I. Shahzadi, M. Ikram, A. Raza, U. Qumar, S. Ali, Appl. Nanosci. 10 (2020) 30007.

[72] A. Gnanaprakasam, V. Sivakumar, M. Thirumarimurugan, Indian J. Mater. Sci. 2015 (2015) 601827.

[73] M. Ikram, A. Raza, M. Imran, A. Ul-Hamid, A. Shahbaz, S. Ali, Nanoscale Res. Lett. 15 (2020) 1.

[74] A. Haider, M. Ijaz, M. Imran, M. Naz, H. Majeed, J. Khan, M. Ali, M. Ikram, Appl. Nanosci. 10 (2020) 1095.

[75] Z. Sabouri, A. Akbari, H.A. Hosseini, M. Khatami, M. Darroudi, Polyhedron 178 (2020) 114351.

[76] K. Kombaiah, J.J. Vijaya, L.J. Kennedy, M. Bououdina, R.J. Ramalingam, H.A. Al-Lohedan, J. Phys. Chem. Solids 115 (2017) 162.

[77] S. Nemati, H.A. Hosseini, A. Hashemzadeh, M. Mohajeri, Z. Sabouri, M. Darroudi, R.K. Oskuee, Mater. Res. Express 6 (2019) 125016.

[78] M. Alikhani, M. Hakimi, K. Moeini, V. Eigner, M. Dusek, J. Inorg. Organomet. Polym. Mater. 30 (2020) 2907.

[79] M. Darroudi, Z. Sabouri, R. Kazemi Oskuee, H. Kargar, H.A. Hosseini, Nanomed. J. 1 (2014) 88.

[80] M. Ahamed, D. Ali, H.A. Alhadlaq, M.J. Akhtar, Chemosphere 93 (2013) 2514.